Phononic second-order topological phase in the C_3N compound

F. F. Huang,[1] P. Zhou,[2] W. Q. Li,[2] S. D. He,[2] R. Tan,[3] Z. S. Ma,[2,*] and L. Z. Sun[1,†]
[1]*Hunan Provincial Key laboratory of Thin Film Materials and Devices, School of Material Sciences and Engineering, Xiangtan University, Xiangtan 411105, China*
[2]*School of Material Sciences and Engineering, Xiangtan University, Xiangtan 411105, China*
[3]*College of Physics and Electronics Engineering, Hengyang Normal University, Hengyang 421002, China*

(Received 24 November 2022; accepted 24 March 2023; published 6 April 2023)

Second-order topological phases in artificial systems have been extensively studied, but studies in the phonons of atomic materials are limited. In this paper, we propose that phononic second-order topological phase exists in C_3N, a previously synthesized and intensively investigated two-dimensional material. Its nontrivial phase arises from the mismatch between the Wannier centers of the out-of-plane phonon modes and the atomic positions. Using a simplified force constant model, we find that gapped edge modes and in-gap corner modes only exist on the structures with broken pure-carbon-ring terminations, and this unexpected phenomenon can be explained by the electronlike filling anomaly for phonons. Further calculations reveal that these corner modes are robust to external disturbances. The nontrivial phononic phase in C_3N provides an avenue in crystalline materials to explore higher-order topological phases in Bose systems.

DOI: 10.1103/PhysRevB.107.134104

I. INTRODUCTION

The discovery of topological insulators have sparked the emergence of many fascinating topological phases. One of the most recent proposals is the higher-order topological insulators (HOTIs). In contrast to conventional topological insulators (first-order topological insulators), in which surface or edge states appear on $(d-1)$-dimensional boundaries, HOTIs host gapless modes on the $(d-n)$-dimensional ($n \geqslant 2$) boundaries [1–27]. Among them, two-dimensional (2D) second-order topological insulators (SOTIs) host zero energy states on the corners. Up to now, they have been reported in various 2D systems, including electrical [28–30], electrical circuits [31,32], acoustic [2,33–38], photonic [15,39–41], and optical systems [42,43].

However, only two all-carbon materials, graphdiyne [44] and α-graphynes [45], have been proposed as phononic SOTIs, and any crystalline material beyond pure carbon materials has not yet been reported. This contrasts with electronic SOTIs, in which many pure carbon and nonpure carbon systems (such as honeycomb antimony [28], 1H transition metal dichalcogenides [46], and black phosphorene [47]) were proposed. The corner modes of a SOTI typically heavily depend on the edge of a structure, and it is not easy to cut a 2D material to a nanostructure with a specific edge. Therefore, the experimental realization of SOTIs in the phonons of realistic materials remains elusive. To this end, it is desirable to identify phononic second-order topological materials that are readily available and highly controllable to their orientations and edges. Here, we suggest that C_3N is a generic phononic SOTI and it has clear advantages over other candidates for the experimental detection of the corner modes. (i) C_3N is the first instance of phononic SOTIs in a material other than pure carbon, suggesting that it would be a great choice to study phononic SOTIs in broader lattices and materials. (ii) Because its out-of-plane modes have three nontrivial wide gaps, the corner modes can maintain their robustness in greater disturbances [5,48], which is intriguing for their potential experimental detection and device applications. (iii) It is a previously synthesized [49,50] and thoroughly studied [51–54] 2D graphenelike atomic material, indicating more potential methods to synthesize and cut the material to a nanostructure with specific edges [55].

With the help of first-principles calculations and a simplified force constant model, we find that C_3N, an experimentally synthesized and intensively investigated carbon-nitrogen materials with honeycomb lattice, can realize the second-order topological phase in out-of-plane phonon modes. Four characteristics of SOTIs are found: quantized finite bulk quadrupole topological number Q_{ij}, quantized secondary topological index $Q^{(6)}{}_{\text{corner}}$, gapped topological edge modes, and in-gap topological corner modes. The gapped edge modes and in-gap corner modes only exist in the structures with broken pure-carbon-ring terminations, which can be explained by the filling anomaly of phonons. Moreover, the robustness of in-gap topological corner modes are identified by importing edge disorders.

II. STRUCTURE AND PHONON SPECTRA

Figure 1(a) shows the C_3N monolayer, with the primitive cell indicated by the red parallelogram. This monolayer can be viewed as nitrogen-doped graphene, with nitrogen atoms taking the place of the two native carbon atoms in

*zsma@xtu.edu.cn
†lzsun@xtu.edu.cn

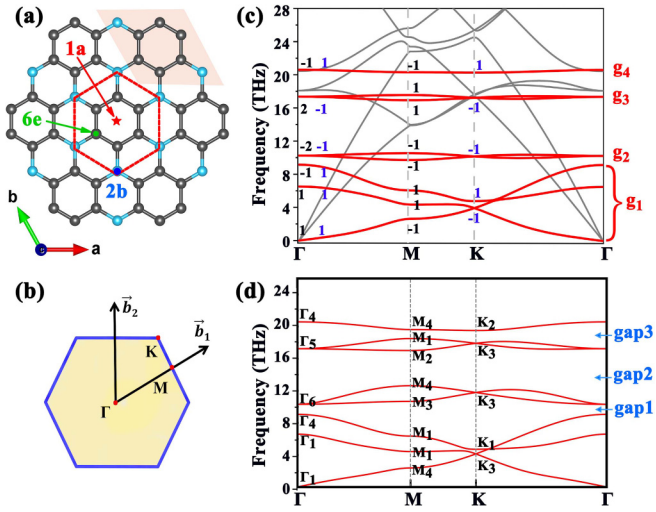

FIG. 1. (a) The atomic structure of C_3N. C and N atoms are represented by the gray and blue balls, respectively. The red shaded area and the red hexagon represent the primitive and Wigner-Seitz cell, respectively. The Wyckoff positions 1a, 2b, and 6e are also shown in this figure. (b) The 2D first Brillouin zone of C_3N. (c) First-principles phonon dispersions of C_3N along the high symmetry lines. The gray and red bands are the in-plane and out-of-plane modes, respectively. Black numbers at the high symmetry points Γ and M are the eigenvalues of C_{2z}, and blue numbers at Γ and K are the eigenvalues of C_{3z}. (d) The phonon dispersion from the simplified force constant (FC) model. The letters at the high symmetry points are the irreps in the subspace *P6mm*, which correspond to the irreps calculated by the first-principles. There are three bandgaps, labeled as gap1, gap2, and gap3, respectively.

a 2×2 supercell of graphene. The space group of C_3N is $P6/mmm$ (No. 191), since we are only interested in the topological properties of out-of-plane modes, it is sufficient to investigate the symmetry properties of these modes under the subgroup of *P6mm* (No. 183) [56]. The C atoms of C_3N occupy Wyckoff position 6e, while the N atoms occupy 2b. The Wigner-Seitz cell is depicted by the hexagon, which clearly exhibits C_6 rotational symmetry. The Wyckoff position of this hexagon's center is 1a. Figure 1(c) and S1 illustrate the phonon spectra of C_3N along the high symmetry path. In the harmonic approximation [56], the out-of-plane (red lines) and in-plane (grey lines) modes are decoupled because their horizontal mirror eigenvalues are even and odd, respectively. Therefore, we can examine the topological characteristics of the two subspaces independently. It is worth noting that similar subspace separation have also been applied for the elastic waves [57], where the corner modes are experimentally observed in the bandgap of the out-of-plane modes, and are unaffected by the "metallic" in-gap in-plane modes. All out-of-plane modes, as shown in Figs. 1(c) and 1(d), can be divided into four groups ($g_1 - g_4$) separated by the phononic band gaps (we call them as gap1, gap2, and gap3 with increasing frequencies).

We build a FC model that accounts for the first to fourth nearest-neighbor interactions to make computations and analysis easier (see Fig. S2 [59]). By fitting the phonon frequencies of C_3N obtained from first-principles calculations, we obtain the parameter values of the FCs (see Table I). The phonon dispersion and the irreducible representations (irreps) of the vibration modes at Γ, K, and M are shown in Fig. 1(d). All of these results are compatible with the first-principles calculations, and the detailed comparison is presented in the Supplementary Materials. Therefore, this model can be used to precisely characterize the out-of-plane modes of C_3N.

TABLE I. Fitted parameter values in the FC model (in units of 10^4 dyn/cm). The nearest-neighbor, next-nearest-neighbor, third-nearest-neighbor, and fourth-nearest-neighbor terms are labeled as 1NN, 2NN, 3NN, and 4NN, respectively.

C-C				C-N			N-N
1NN	2NN	3NN	4NN	1NN	2NN	4NN	3NN
−91.45	−0.13	0.09	−1.86	−49.00	11.82	7.26	−13.71

III. NONTRIVIAL TOPOLOGICAL PROPERTIES

Phonons are typical bosons whose occupations are not restricted by the Pauli exclusion principle. Therefore, they are detectable across all frequency ranges, and one can define a topological invariant for any group of isolated bands. Then the issue is what topological invariant can be employed to describe its nontrivial features. In quantum Hall or quantum anomalous Hall effects, the Chern number is used to characterize the topology of bands [60]. In the C_3N system, however, it is zero because of the coexistence of time reversal and inversion symmetries [61]. Z_2 is also trivial because no typical features, such as band inversion near the Fermi level, occur. In addition, due to the existence of C_6 rotational symmetry, the total bulk dipole moment of the system is zero [62]. Hence we will investigate the quadrupole topological number from the bulk dipole moment as [4,62]

$$Q_{ij} = \frac{1}{2}\left(\sum_n 2p_i^n p_j^n \bmod 2\right), \tag{1}$$

where the summation is over all the bands below a bulk gap, i and j are the directions of reciprocal lattice vectors, and p_i^n is the bulk dipole moment of the nth band in the i direction. Under C_6 rotational symmetry, $p_i^n = p_j^n$ and it can be obtained from

$$p_i^n = \frac{1}{2}\left(q_i^n \bmod 2\right), \quad (-1)^{q_i^n} = \frac{\eta^n(M)}{\eta^n(\Gamma)}, \tag{2}$$

where η^n is the parity of the nth band at the corresponding k point (M or Γ), and they have the opposite sign to the eigenvalues of C_{2z} [63]. According to the eigenvalues of C_{2z} in Fig. 1(c), the quadrupole topological numbers for the lowest three, five, and seven bands are 1/2. These fractional quadrupole topological numbers indicate that the three band gaps are topologically nontrivial.

In the previous studies, despite the fact that they both host fractional corner states, some nontrivial HOTIs originate from quantized quadrupole moments and others from the filling anomaly [64]. The topological invariant of the latter is the secondary topological index. We further examine this index for 0D hexagonal C_3N nanodisk. For a C_6-symmetric crystal,

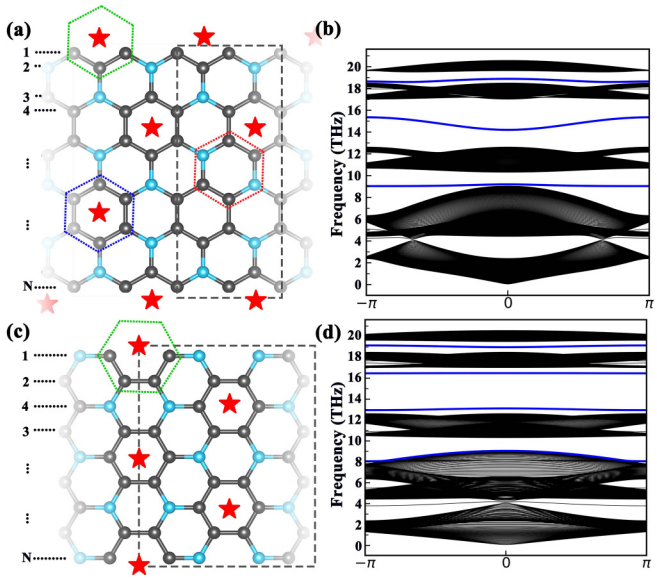

FIG. 2. There are two types of hexagonal atomic rings in C_3N. One type, as denoted by the red dashed hexagons, consists of C-C bonds and C-N bonds, is called a C-N ring. The other type indicated by the blue hexagon only consists of C-C bonds, is called a pure-carbon ring. The green hexagons indicate the broken pure-carbon rings. (a) The zigzag-edged 1D atomic structure with broken pure-carbon-ring terminations. The grey dashed rectangle represents its unitcell. The stars denote the Wyckoff position 1a. (b) Corresponding phonon spectrum of (a). The phonon spectrums denoted by blue lines are topological edge modes, and denoted by black lines are projected bulk modes. There are three bandgaps between the projected bulk modes, we call them gap1, gap2, and gap3 with increasing frequencies. (c), (d) Same as (a), (b) but the 1D structure is armchair-edged.

the secondary topological index is given by [65]

$$Q^{(6)}{}_{\text{corner}} = \tfrac{1}{4}\left[M_1^{(2)}\right] + \tfrac{1}{6}\left[K_1^{(3)}\right] \mod 1, \tag{3}$$

where $[M_1^{(2)}]$ ($[K_1^{(3)}]$) is the difference in the number of the occupied bands with $\hat{C}_2$ ($\hat{C}_3$) eigenvalue 1 between Γ and M (Γ and K). Here we regard the phonon bands below a gap as "occupied bands". These eigenvalues of the phonon spectra in C_3N are shown in Fig. 1(c). For each of the three gaps, the $[M_1^{(2)}]$ ($[K_1^{(3)}]$) share the same values of

$$\left[M_1^{(2)}\right] = 0, \quad \left[K_1^{(3)}\right] = -2. \tag{4}$$

Accordingly, the secondary topological indexes of the three gaps are $\frac{1}{3}$. We will go into more detail about it later. The results above show that both of the fractional secondary topological index and the fractional quadrupole topological number can be used to explain the topological origin of the higher-order topological phononic phase in C_3N.

IV. NONTRIVIAL EDGE AND CORNER MODES

A fascinating property of a SOTI is its nontrivial edge and corner modes. As shown in Fig. S3 [59], there are four different types of edges if you cut C_3N into nanoribbons. After calculating the phonon bands of these nanoribbons in 1D Brillouin zone, we find only two of them, as shown in Fig. 2, host nontrivial edge modes, which (blue lines) locate between the projected bulk bands in the frequency ranges of gap1, gap2, and gap3. The edge modes in gap1, however, merge into the projected bulk modes because the value of gap1 is too small. It is important to note that due to different unitcell sizes, in gap2, there are two edge states for armchair edges and one edge state for zigzag edges (see details in the Supplementary Materials [59]). Next, we investigate the corner modes of C_3N nanodisk. Figure 3(a) shows the atomic structure of a nanodisk with the armchair edges. The phonon eigenfrequencies of the structure are obtained by diagonalizing the FC Hamiltonian in momentum space. As shown in Fig. 3(b), corner modes exist in all of the three gaps and their frequencies separate from the projected bulk modes and edge modes. Since the value of gap1 is small, the corresponding edge modes merge into the projected bulk modes. The corner modes in gap1, gap2, and gap3 have frequencies of 9.14 THz, 14.86 THz, and 18.68 THz, respectively. Figure 3(e) shows the real-space wavefunction distributions. They obey C_6 rotational symmetry and are localized at the corners of the nanodisk.

Their nontrivial edge and corner modes can be explained by the theory of elementary band representations (EBR) [56,66,67]. Following the paper of Juan L. Mañes [56], a mechanical band representation can be labeled by V@w, where V is a representation of site point group and w is a Wyckoff position. For C_3N, C and N atoms occupy the Wyckoff positions 6e (0.167, 0.833, 0.0) and 2b (0.667, 0.333, 0.0), respectively. The induced irreps of the out-of-plane vibrations at these positions are presented in Table II. 2b is maximal but 6e is not. The induced band representations from 6e must be composite. According to the EBR of space group *P6mm*, the mechanical band representations of g_2, g_3, g_4 can be regarded as the induced representation from the local site representation E_1, E_2, B_1, respectively, and the mechanical band representation of g_1 can be seen as the sum of the induced representation of A_1 in 1a and A_1 in 2b:A_1@1a $\oplus$ A_1@2b. However, the atoms of the C_3N structure do not place in 1a, so a mismatch happens for the EBR of A_1@1a. Therefore, the mismatch between atomic positions and the Wannier centers of phonons produce a kind of filling anomaly [65,68], which can also be used to explain the termination-dependent edge modes. For the C_3N ribbons with broken pure-carbon-ring terminations [see Figs. 2(a) and 2(c)], the atoms in real space and the vibration modes in reciprocal space are unbalanced, which makes the energies of the edge modes deriving from the edge Wannier centers different from the energies of projected bulk modes.

V. ROBUSTNESS AGAINST DISORDERS

Because of SOTI's nontrivial quadrupole topological number, topologically protected corner modes are robust against disorders as long as the bulk or edge gaps are not closed [5]. The disorders may come from edge external atomic adsorption, edge defects, or other factors. Here we simulate these situations by introducing random hopping terms into the edge atoms and then numerically evaluating their corner modes as well as their real-space wave function distributions. For the edge atoms, we add random self FC ranging from −1.69 to 1.69 THz, with the value 1.69 THz being almost half of the values of gap2 [28]. The simulations are repeated 500 times, and the average eigenfrequencies are plotted in Figs. 4(a)–(d). As shown in Figs. 4(c) and 4(d), the corner

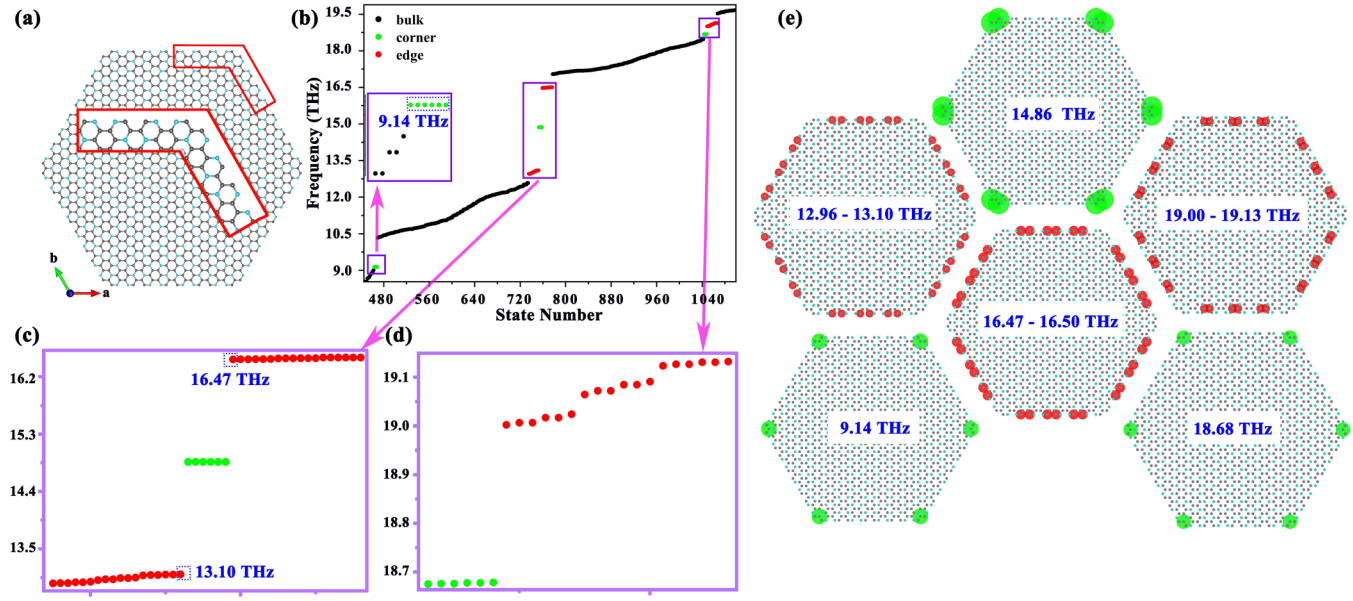

FIG. 3. (a) The hexagonal atomic structure of armchair-edged C_3N with broken pure-carbon-ring terminations. (b) Numerically evaluated eigenfrequencies of structure (a). Black, green, and red dots denote bulk, topological corner, and gapped edge modes, respectively. There are three bandgaps between the bulk modes, we call them gap1, gap2, and gap3 with increasing frequencies. (c), (d) The corresponding enlarged view of modes in the highest and middle bulk gaps. (e) The real-space wave function distributions at a particular frequency or range.

modes in gap2 and gap3 are localized and separated from the edge modes. Furthermore, we investigated the average real-space wave function distributions of modes ranging from 14.82 to 14.91 THz (the frequency range of the corner modes in gap2) and from 18.65 to 18.71 THz (the frequency range of the corner modes in gap3), the results are shown in Figs. 4(e) and 4(f), respectively. We discover that the corner modes still concentrate around the corners and the edge disorders do not destroy them.

VI. DISCUSSION

In summary, we propose that experimentally synthesized C_3N host nontrivial phononic second-order topological phase. In the subspace of out-of-plane modes, three nontrivial band gaps with fractional quadrupole topological number and secondary topological index are discovered. Its edge and corner modes rely on edge terminations; the nontrivial boundary modes only exist on the boundaries with broken pure-carbon rings. A detailed EBR analysis reveals that these edge modes result from the electronlike filling anomaly for the phonons. The nontrivial topology of C_3N is further validated by its nontrivial corner modes, which are robust against edge disorders.

According to the transmission electron microscopy images in Refs. [49,50], hexagonal C_3N nanodisks can be obtained from different synthesis methods, which will greatly facilitate the experimental observation of phononic corner modes. The synthesized nanodisks can be further handled by some top-down strategies, such as etching method [55], to obtain the nanodisks with particular edges. Regarding the experimental observation of the corner modes, the symmetry analysis reveals that the irreducible representations for these modes are $B_{2g} + E_{1g} + A_{2u} + E_{2u}$. The A_{2u} mode is infrared active, and E_{1g} mode is Raman active (see details in the Supplementary Materials [59]). Hence, the phononic corner modes can be verified by stimulating them with infrared or Raman light, and their frequencies can serve as a guide for detection in future experiments. Since the corner modes are spatially concentrated around the corners, it is also possible to identify

TABLE II. The first five rows (except for the seventh column) are part of EBRs induced from irreps of the maximal site-symmetry groups in *P6mm* (No. 183). The data is available on the Bilbao Crystallographic Server [58]. The first row lists the Wyckoff positions, the point groups isomorphic to their site-symmetry groups are presented in the parentheses. The second row gives the irreps of the site-symmetry groups corresponding to the out-of-plane modes, from which the band representation is induced. The third, fourth, and fifth rows give the little group representations that appear in the induced EBR. The dimension of the EBR, which is also the connectivity of the elementary band rep, is given in the parentheses. The sixth row is the labels of band groups in the out-of-plane modes of C_3N.

Wyckoff	1a(C_{6v})	2b(C_{3v})	1a(C_{6v})	1a(C_{6v})	1a(C_{6v})	6e(C_s)
ρ	A_1	A_1	E_1	E_2	B_1	A'
$\Gamma(0,0,0)$	$\Gamma_1(1)$	$\Gamma_1(1) \oplus \Gamma_4(1)$	$\Gamma_6(2)$	$\Gamma_5(2)$	$\Gamma_4(1)$	$\Gamma_1(1) \oplus \Gamma_4(1) \oplus \Gamma_5(2) \oplus \Gamma_6(2)$
$K(\frac{1}{3}, \frac{1}{3}, 0)$	$K_1(1)$	$K_3(2)$	$K_3(2)$	$K_3(2)$	$K_2(1)$	$K_1(1) \oplus K_2(1) \oplus 2K_3(2)$
$M(\frac{1}{2}, 0, 0)$	$M_1(1)$	$M_1(1) \oplus M_4(1)$	$M_3(1) \oplus M_4(1)$	$M_1(1) \oplus M_2(1)$	$M_4(1)$	$2M_1(1) \oplus M_2(1) \oplus M_3(1) \oplus 2M_4(1)$
Band group		g_1	g_2	g_3	g_4	

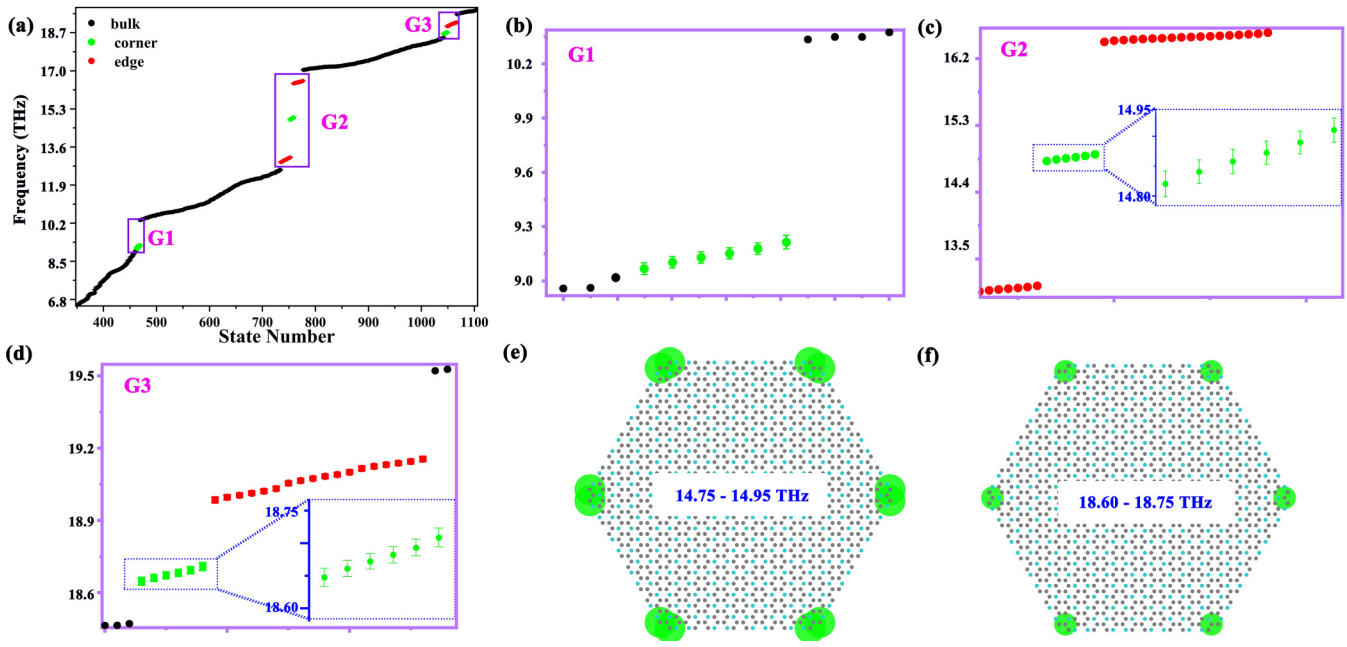

FIG. 4. Average frequencies distributions of modes with respect to random hopping terms added to the edge atoms. The bulk, edge, and corner modes are colored by black, red, and green, respectively. (a) Numerically evaluated averaged eigenfrequencies. (b)-(d) Enlarged views of the average frequency distributions in gap1, gap2, and gap3, respectively. The dots are the mean values of frequencies for each mode, the error bar represents standard deviation of the mean values. (e), (f) Average real-space wavefunction distributions of modes with ranges 14.75–14.95 THz and 18.60–18.75 THz, respectively.

corner modes from bulk or edge modes using some space-resolved experimental techniques. The transport properties of the corner modes can be studied by adding two "leads" around a corner [69], as shown in Fig. S6 of the Supplementary Materials [59]. Nowadays, two common methods are used to measure the thermal conductivity of 2D materials: the optothermal Raman technique and the microbridge method. Here we can refer to the microbridge method to study the transport of the corner modes in C_3N. Because the frequencies of out-of-plane corner modes differ from the frequencies of corresponding edge and bulk modes, if the two leads are close enough to the corners, the contribution of the corner modes dominates the thermal transport. Moreover, the structure can also be used to theoretically investigate the transport properties of corner states with quantum mechanical calculations of three-phonon scattering rates within the framework of the Peierls-Boltzmann transport theory or classical molecular dynamics simulations [70] (See the details in the Supplementary Materials [59]). Recently, the nontrivial thermal corner states have been demonstrated in a generalized 2D diffusion lattice [71] and the corner states can be observed because of the anti-Hermitian nature of the diffusion Hamiltonian, and they have been proved to be robust against local or global defects. This pioneering experiment provides the basic idea for the future observation of thermal corner states in crystalline materials.

ACKNOWLEDGMENTS

This work is supported by the National Natural Science Foundation of China (Grants No. 11804287 and No. 11872054), Hunan Provincial Natural Science Foundation of China (Grants No. 2019JJ50577, No. 2021JJ30686, No. 2022JJ40008, and No. 2020JJ2026), Scientific Research Fund of Hunan Provincial Education Department (Grant No. 18A051), the Postgraduate Scientific Research Innovation Project of Hunan Province (Grant No. QL20210143), the Postgraduate Scientific Research Innovation Project of Xiangtan University (Grant No. XDCX2021B131), and Scientific Research Fund of Hunan Provincial Education Department (Grant No. 21C0549).

[1] W. A. Benalcazar, B. A. Bernevig, and T. L. Hughes, Science **357**, 61 (2017).
[2] Y. Yang, J. Lu, M. Yan, X. Huang, W. Deng, and Z. Liu, Phys. Rev. Lett. **126**, 156801 (2021).
[3] Q. Wei, X. Zhang, W. Deng, J. Lu, X. Huang, M. Yan, G. Chen, Z. Liu, and S. Jia, Nat. Mater. **20**, 812 (2021).
[4] W. A. Benalcazar, B. A. Bernevig, and T. L. Hughes, Phys. Rev. B **96**, 245115 (2017).
[5] J. Langbehn, Y. Peng, L. Trifunovic, F. von Oppen, and P. W. Brouwer, Phys. Rev. Lett. **119**, 246401 (2017).
[6] Z. Song, Z. Fang, and C. Fang, Phys. Rev. Lett. **119**, 246402 (2017).
[7] F. Schindler, A. M. Cook, M. G. Vergniory, Z. Wang, S. S. P. Parkin, B. A. Bernevig, and T. Neupert, Sci. Adv. **4**, eaat0346 (2018).
[8] M. Geier, L. Trifunovic, M. Hoskam, and P. W. Brouwer, Phys. Rev. B **97**, 205135 (2018).

[9] S. Qian, G.-B. Liu, C.-C. Liu, and Y. Yao, Phys. Rev. B **105**, 045417 (2022).

[10] Z. Guo, J. Deng, Y. Xie, and Z. Wang, npj Quantum Mater. **7**, 87 (2022).

[11] Z. H. Li, P. Zhou, Q. H. Yan, X. Y. Peng, Z. S. Ma, and L. Z. Sun, Phys. Rev. B **106**, 085126 (2022).

[12] F. Schindler, Z. Wang, M. G. Vergniory, A. M. Cook, A. Murani, S. Sengupta, A. Y. Kasumov, R. Deblock, S. Jeon, I. Drozdov *et al.*, Nat. Phys. **14**, 918 (2018).

[13] Y. Xu, Z. Song, Z. Wang, H. Weng, and X. Dai, Phys. Rev. Lett. **122**, 256402 (2019).

[14] R.-X. Zhang, F. Wu, and S. Das Sarma, Phys. Rev. Lett. **124**, 136407 (2020).

[15] S. Mittal, V. V. Orre, G. Zhu, M. A. Gorlach, A. Poddubny, and M. Hafezi, Nat. Photonics **13**, 692 (2019).

[16] F. Zhang, C. L. Kane, and E. J. Mele, Phys. Rev. Lett. **110**, 046404 (2013).

[17] S. Qian, C.-C. Liu, and Y. Yao, Phys. Rev. B **104**, 245427 (2021).

[18] K. Kudo, T. Yoshida, and Y. Hatsugai, Phys. Rev. Lett. **123**, 196402 (2019).

[19] Z. Su, Y. Kang, B. Zhang, Z. Zhang, and H. Jiang, Chin. Phys. B **28**, 117301 (2019).

[20] A. Cerjan, M. Jürgensen, W. A. Benalcazar, S. Mukherjee, and M. C. Rechtsman, Phys. Rev. Lett. **125**, 213901 (2020).

[21] Z.-Z. Yang, X. Li, Y.-Y. Peng, X.-Y. Zou, and J.-C. Cheng, Phys. Rev. Lett. **125**, 255502 (2020).

[22] M. J. Park, Y. Kim, G. Y. Cho, and S. B. Lee, Phys. Rev. Lett. **123**, 216803 (2019).

[23] B. Liu, L. Xian, H. Mu, G. Zhao, Z. Liu, A. Rubio, and Z. F. Wang, Phys. Rev. Lett. **126**, 066401 (2021).

[24] H. Huang, J. Fan, D. Li, and F. Liu, Nano Lett. **21**, 7056 (2021).

[25] H. Li and K. Sun, Phys. Rev. Lett. **124**, 036401 (2020).

[26] R. Chen, C.-Z. Chen, J.-H. Gao, B. Zhou, and D.-H. Xu, Phys. Rev. Lett. **124**, 036803 (2020).

[27] C.-H. Hsu, P. Stano, J. Klinovaja, and D. Loss, Phys. Rev. Lett. **121**, 196801 (2018).

[28] S. K. Radha and W. R. L. Lambrecht, Phys. Rev. B **102**, 115104 (2020).

[29] C. Chen, Z. Song, J.-Z. Zhao, Z. Chen, Z.-M. Yu, X.-L. Sheng, and S. A. Yang, Phys. Rev. Lett. **125**, 056402 (2020).

[30] Q.-B. Zeng, Y.-B. Yang, and Y. Xu, Phys. Rev. B **101**, 241104(R) (2020).

[31] J. Wu, X. Huang, J. Lu, Y. Wu, W. Deng, F. Li, and Z. Liu, Phys. Rev. B **102**, 104109 (2020).

[32] S. Liu, W. Gao, Q. Zhang, S. Ma, L. Zhang, C. Liu, Y. J. Xiang, T. J. Cui, and S. Zhang, Research **2019**, 8609875 (2019).

[33] Z.-G. Chen, C. Xu, R. Al Jahdali, J. Mei, and Y. Wu, Phys. Rev. B **100**, 075120 (2019).

[34] H. Xue, Y. Yang, F. Gao, Y. Chong, and B. Zhang, Nat. Mater. **18**, 108 (2019).

[35] X. Ni, M. Weiner, A. Alu, and A. B. Khanikaev, Nat. Mater. **18**, 113 (2019).

[36] X. Zhang, H.-X. Wang, Z.-K. Lin, Y. Tian, B. Xie, M.-H. Lu, Y.-F. Chen, and J.-H. Jiang, Nat. Phys. **15**, 582 (2019).

[37] Y. Qi, C. Qiu, M. Xiao, H. He, M. Ke, and Z. Liu, Phys. Rev. Lett. **124**, 206601 (2020).

[38] X. Huang, J. Lu, Z. Yan, M. Yan, W. Deng, G. Chen, and Z. Liu, Sci. Bull. **67**, 488 (2022).

[39] J. Noh, W. A. Benalcazar, S. Huang, M. J. Collins, K. P. Chen, T. L. Hughes, and M. C. Rechtsman, Nat. Photonics **12**, 408 (2018).

[40] X.-D. Chen, W.-M. Deng, F.-L. Shi, F.-L. Zhao, M. Chen, and J.-W. Dong, Phys. Rev. Lett. **122**, 233902 (2019).

[41] B.-Y. Xie, H.-F. Wang, H.-X. Wang, X.-Y. Zhu, J.-H. Jiang, M.-H. Lu, and Y.-F. Chen, Phys. Rev. B **98**, 205147 (2018).

[42] G. Pelegrí, A. M. Marques, V. Ahufinger, J. Mompart, and R. G. Dias, Phys. Rev. B **100**, 205109 (2019).

[43] Y. Lei, X.-W. Luo, and S. Zhang, Opt. Express **30**, 24048 (2022).

[44] H. Mu, B. Liu, T. Hu, and Z. Wang, Nano. Lett. **22**, 1122 (2022).

[45] J. Zhu, W. Wu, J. Zhao, C. Chen, Q. Wang, X.-L. Sheng, L. Zhang, Y. X. Zhao, and S. A. Yang, Phys. Rev. B **105**, 085123 (2022).

[46] J. Zeng, H. Liu, H. Jiang, Q.-F. Sun, and X. C. Xie, Phys. Rev. B **104**, L161108 (2021).

[47] M. Hitomi, T. Kawakami, and M. Koshino, Phys. Rev. B **104**, 125302 (2021).

[48] E. Khalaf, Phys. Rev. B **97**, 205136 (2018).

[49] S. Yang, W. Li, C. Ye, G. Wang, H. Tian, C. Zhu, P. He, G. Ding, X. Xie, Y. Liu *et al.*, Adv. Mater. **29**, 1605625 (2017).

[50] J. Mahmood, E. K. Lee, M. Jung, D. Shin, H.-J. Choi, J.-M. Seo, S.-M. Jung, D. Kim, F. Li, M. S. Lah *et al.*, Proc. Natl. Acad. Sci. USA **113**, 7414 (2016).

[51] Z. Li and F. Cheng, Physica E: Low Dimens. Syst. Nanostruct. **124**, 114320 (2020).

[52] J. Xu, J. Mahmood, Y. Dou, S. Dou, F. Li, L. Dai, and J.-B. Baek, Adv. Mater. **29**, 1702007 (2017).

[53] P. Thaddeus, C. Gottlieb, H. Gupta, S. Brünken, M. McCarthy, M. Agúndez, M. Guélin, and J. Cernicharo, Astrophys. J. **677**, 1132 (2008).

[54] A. Bafekry, S. Farjami Shayesteh, and F. M. Peeters, J. Phys. Chem. C **123**, 12485 (2019).

[55] T. Zhang, S. Wu, R. Yang, and G. Zhang, Front. Phys. **12**, 1 (2017).

[56] J. L. Mañes, Phys. Rev. B **102**, 024307 (2020).

[57] H. Fan, B. Xia, L. Tong, S. Zheng, and D. Yu, Phys. Rev. Lett. **122**, 204301 (2019).

[58] M. I. Aroyo, A. Kirov, C. Capillas, J. Perez-Mato, and H. Wondratschek, Acta Crystallogr. Sect. A **62**, 115 (2006).

[59] See Supplemental Material at http://link.aps.org/supplemental/10.1103/PhysRevB.107.134104 for (1) phonon dispersion from first-principles calculation, (2) details of the force constant model, (3) C_3N ribbons with four different edges, (4) comparison of edge modes between two different C_3N nanoribbons with unitcells containing the same number of edge atoms, (5) symmetry analysis of the raman and infrared active corner modes, and (6) a suggestion to calculate or measure the thermal conductivity of the corner modes.

[60] Y. Liu, Y. Xu, S.-C. Zhang, and W. Duan, Phys. Rev. B **96**, 064106 (2017).

[61] D. Xiao, M.-C. Chang, and Q. Niu, Rev. Mod. Phys. **82**, 1959 (2010).

[62] B. Liu, G. Zhao, Z. Liu, and Z. Wang, Nano Lett. **19**, 6492 (2019).
[63] F. Liu, H.-Y. Deng, and K. Wakabayashi, Phys. Rev. Lett. **122**, 086804 (2019).
[64] B. Xie, H.-X. Wang, X. Zhang, P. Zhan, J.-H. Jiang, M. Lu, and Y. Chen, Nat. Rev. Phys. **3**, 520 (2021).
[65] W. A. Benalcazar, T. Li, and T. L. Hughes, Phys. Rev. B **99**, 245151 (2019).
[66] B. Bradlyn, L. Elcoro, M. G. Vergniory, J. Cano, Z. Wang, C. Felser, M. I. Aroyo, and B. A. Bernevig, Phys. Rev. B **97**, 035138 (2018).
[67] J. Cano, B. Bradlyn, Z. Wang, L. Elcoro, M. G. Vergniory, C. Felser, M. I. Aroyo, and B. A. Bernevig, Phys. Rev. B **97**, 035139 (2018).
[68] M. Ezawa, Phys. Rev. Lett. **120**, 026801 (2018).
[69] K.-T. Wang, Y. Ren, F. Xu, Y. Wei, and J. Wang, Sci. China Phys. Mech. Astron. **64**, 257811 (2021).
[70] X. Gu and R. Yang, Annu. Rev. Heat Transfer **16**, 1 (2016).
[71] H. Wu, H. Hu, X. Wang, Z. Xu, B. Zhang, Q. J. Wang, Y. Zheng, J. Zhang, T. J. Cui, and Y. Luo, Adv. Mater. 2210825 (2023).